Linear and Nonlinear Mass Sensing Using Piezoelectrically-Actuated Microcantilevers

Conference Paper · March 2011

DOI: 10.1007/978-1-4419-8825-6_9

7 authors, including:

Vijay Kumar
University of Duisburg-Essen
63 PUBLICATIONS **492** CITATIONS
SEE PROFILE

John Boley
Boston University
25 PUBLICATIONS **386** CITATIONS
SEE PROFILE

George T.-C. Chiu
Purdue University
222 PUBLICATIONS **3,183** CITATIONS
SEE PROFILE

Jeffrey F Rhoads
Purdue University
106 PUBLICATIONS **1,242** CITATIONS
SEE PROFILE

Proceedings of the SEM Annual Conference
June 7-10, 2010 Indianapolis, Indiana USA

Linear and Nonlinear Mass Sensing Using Piezoelectrically-Actuated Microcantilevers

Vijay Kumar[1,2,3,*], J. William Boley[1], Hendrik Ekowaluyo[1,2], Jacob K. Miller[1,2,3]
George C. Marvin[1,2], George T.-C. Chiu[1,2,3], Jeffrey F. Rhoads[1,2,3]

[1] *School of Mechanical Engineering, Purdue University, West Lafayette, IN 47907*

[2] *Birck Nanotechnology Center, Purdue University, West Lafayette, IN 47907*

[3] *Ray W. Herrick Laboratories, Purdue University, West Lafayette, IN 47907*

[*] *Corresponding author: kumar2@purdue.edu*

Abstract

Chemical and biological sensors based on resonant microcantilevers offer distinct utility due to their small size, low power consumption, high sensitivity, and, when bulk fabricated, comparatively-low cost. Modern resonant mass sensors typically utilize chemomechanically-induced frequency shifts in linear resonators for analyte detection. Recent results, however, have indicated that nonlinear sensors, which actively exploit dynamic transitions across sub-critical or saddle-node bifurcations in the device's frequency response, have the potential to exhibit improved performance metrics and operate effectively at smaller scales. This relatively-novel sensing approach directly exploits chemomechanically-induced amplitude shifts, instead of frequency shifts, for detection. Accordingly, it has the potential to eliminate the need for numerous power-consuming signal processing components in final sensor implementations. The present work details the ongoing development of low-cost, linear and nonlinear, bifurcation-based mass sensors founded upon selectively-functionalized, piezoelectrically-actuated microcantilevers. Specifically, the work describes the modeling, analysis, micro-inkjet functionalization, and experimental characterization of these devices.

1 Introduction

Chemical and biological sensors based on resonant micro- and nanocantilevers offer distinct utility due to their small size, low power consumption, high sensitivity, and, when bulk fabricated, comparatively-low cost (see, for example, [1–6]). Collectively, these benefits have spurred the implementation of resonant micro- and nanosensors in medical diagnostic, environmental safety, and national security settings [7–11]. Though a number of transduction mechanisms have been utilized for small-scale mass sensing, piezoelectrically-actuated microcantilevers have garnered significant interest of late, due to their self-sensing capability [12] and maturity in the related technical areas of force sensing and scanning probe microscopy [13]. The study detailed herein seeks to build upon prior research in each of the aforementioned areas with the development of nonlinear, bifurcation-based mass sensors based on piezoelectrically-actuated microcantilevers.

Traditionally, resonant mass sensors have exploited shifts in a linear resonator's natural frequency for analyte detection [see Fig. 1(a)]. In these devices, the adsorption/absorption of a target analyte onto a selectively-functionalized surface layer results in a measurable change in the system's mass (or stiffness). This, in turn, leads to a measurable change in the resonator's natural frequency, which can be directly correlated to an analyte detection event, and, in certain cases, used to approximate the analyte's relative concentration in the test environment [1]. While this linear sensing approach offers proven utility, recent work has demonstrated that improved sensor metrics may be achievable through the active exploitation of nonlinear system behaviors. Dai et al., for example, highlighted the benefits of resonant mass sensors that utilize shifts in the system's nonlinear resonant frequency for detection [14]. Likewise, Younis and Alsaleem recently investigated an amplitude shift based sensing system which leverages the pull-in dynamics of electrostatically-actuated microresonators to realize improved performance [15]. These nonlinear approaches have particular appeal as they are not only functional at the microscale, but potentially facilitate resonant sensing in nanowire and nanotube-based systems, which commonly suffer from a limited linear dynamic range [16].

The present work details the ongoing development of linear and nonlinear mass sensors based on piezoelectrically-actuated microresonators. The latter sensors, described at length in Section 2.1, are founded upon a novel bifurcation-based sensing approach, which utilizes amplitude shifts resulting from chemomechanically-induced dynamic transitions across saddle-node bifurcations to signal analyte detection [see Fig. 1(b)]. The work begins with the development of a

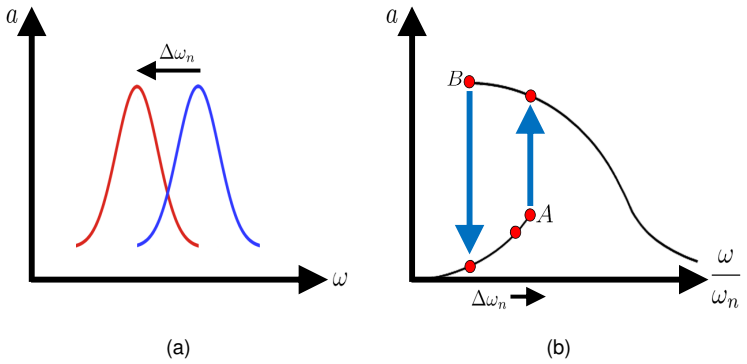

Figure 1: (a) Linear frequency response associated with a representative piezoelectrically-actuated microresonator. Here a chemomechanical interaction between the sensor and a target analyte, induces a measurable frequency shift. (b) Nonlinear frequency response associated with a representative piezoelectrically-actuated microresonator plotted in terms of the system's normalized excitation frequency. Note that a small shift in the system's natural frequency, caused by a chemomechanical interaction between the sensor and a target analyte, drives the system across the saddle-node bifurcation, inducing a dynamic transition between the co-existing stable states. The dramatic increase in response amplitude attendant to this transition can be directly correlated to an analyte detection event.

comprehensive nonlinear, distributed-parameter model for a piezoelectrically-actuated microcantilever. This model is reduced to a lumped-mass analog and subsequently analyzed using numerical continuation methods. Predicted nonlinear behaviors are experimentally validated using Veeco DMASP probes. These devices are functionalized for sensing purposes and tested in an a controlled environment. The work concludes with a brief summary and an overview of ongoing research efforts.

2 Modeling and Analysis

Figure 2 highlights, schematically and pictorially, the piezoelectrically-actuated microbeam system of interest. Here, an applied potential across the system's piezoelectric layer serves to actuate the device. The equation of motion governing the piezoelectrically-actuated microbeam can be recovered through the use of classical energy methods. Though a complete derivation of this governing equation is beyond the scope of the present work, it can be briefly developed as follows.

To begin, axial and transverse deformations $u(s,t)$ and $v(s,t)$, and the derivative operators $(\dot{\bullet})$ and $(\bullet)'$, taken with respect to time and the arc length variable s, respectively, are introduced. Assuming small (but not necessarily linear) deflections, these deformations render a kinematic constraint on the microbeam's angular deflection (ψ) given by

$$\tan\psi = \frac{v'}{1+u'}. \tag{1}$$

Likewise, the axial strain associated with the microbeam, ε_{11}, is given by

$$\begin{aligned} \varepsilon_{11} &= -(y-y_n)\psi' \quad \text{for} \quad s < l_1, \\ &= -y\psi' \qquad\quad \text{for} \quad l_1 < s < l, \end{aligned} \tag{2}$$

where, y_n is the location of neutral axis from the origin for the region $s < l_1$ and is defined to be

$$y_n = \frac{E_p w_p t_p (t_p + t_b)}{2(E_p t_p w_p + E_b t_b w_b)}. \tag{3}$$

The relationships between the induced stress and the strain in the silicon cantilever and the piezoelectric patch are derived using classical constitutive relations. For the cantilever, the constitutive equation is given by $\sigma_{11}^b = E_b \varepsilon_{11}^b$, while, for the piezoelectric patch, the constitutive relations are given by [17, 18]

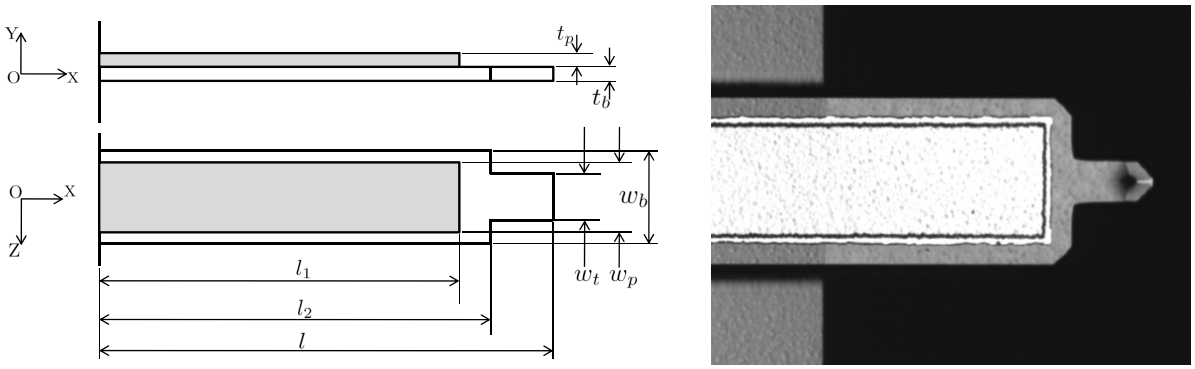

(a) (b)

Figure 2: (a) Schematic of the piezoelectrically-actuated microcantilever. (b) A representative piezoelectrically-actuated Veeco DMASP probe.

$$\begin{aligned}\sigma_{11}^p &= E_p\varepsilon_{11}^p - h_{31}Q_3 + \frac{\alpha_1}{2}(\varepsilon_{11}^p)^2 + \frac{\alpha_2}{2}(Q_3)^2 - \alpha_3\varepsilon_{11}^p Q_3,\\ D_3 &= h_{31}\varepsilon_{11}^p + \beta_{31}Q_3 + \frac{\alpha_3}{2}(\varepsilon_{11}^p)^2 + \frac{\alpha_4}{2}(Q_3)^2 - \alpha_2\varepsilon_{11}^p Q_3,\end{aligned} \tag{4}$$

where, the superscripts b and p denote the beam and the piezoelectric patch, respectively, and σ_{11}, E_b, E_p, Q_3, D_3, h_{31} and β_{31} represent the axial stress, the elastic modulus of the beam, the elastic modulus of the piezoelectric material, the applied electric field, the electrical displacement, the effective coupling coefficient that relates the electrical and mechanical displacements, and the effective permittivity coefficient, respectively. α_i ($i = 1, 2, 3, 4$) are the nonlinear material coefficients. Note that the electric field is the gradient of the applied potential with respect to the thickness variable.

Using the aforementioned relationships, the kinetic energy T and the potential energy U associated with the system can be expressed as

$$T = \frac{1}{2}\int_0^l m(s)\left[\dot{u}^2 + \dot{v}^2\right]\mathrm{d}s, \tag{5}$$

$$\begin{aligned}U =& \frac{1}{2}\int_0^{l_1}\iint_A \sigma_{11}^p\varepsilon_{11}^p \mathrm{d}A\mathrm{d}s + \frac{1}{2}\int_0^{l_1}\iint_A \sigma_{11}^b\varepsilon_{11}^b \mathrm{d}A\mathrm{d}s - \frac{1}{2}\int_0^{l_1}\iint_A Q_3 D_3 \mathrm{d}A\mathrm{d}s\\ &+ \frac{1}{2}\int_{l_1}^{l_2}\iint_A \sigma_{11}^b\varepsilon_{11}^b \mathrm{d}A\mathrm{d}s + \frac{1}{2}\int_{l_2}^{l}\iint_A \sigma_{11}^b\varepsilon_{11}^b \mathrm{d}A\mathrm{d}s,\end{aligned} \tag{6}$$

where $m(s)$ and A represent the mass density and cross-sectional area of the composite system. Using these as a basis for study, the Lagrangian of the system can be assembled and used in conjunction with extended Hamilton's principle to recover the equations governing the system's transverse and longitudinal vibrations. The equation governing the system's longitudinal dynamics can be use to recover the embedded Lagrange multiplier, introduced to maintain inextensibility. Substituting this expression into the equation governing transverse vibrations yields a single, distributed-parameter equation of motion for the system. Expanding this equation, retaining terms of up to third order, and non-dimensionalzing the result, renders a final distributed parameter model.

The complex distributed-parameter model referred to above can be reduced to a lumped-mass analog by decomposing the transverse displacement $\hat{v}$ into its spatial and temporal components

$$\hat{v}(\hat{s}, \hat{t}) = w(\hat{t})\Phi(\hat{s}), \tag{7}$$

and projecting the result onto the first mode shape of the cantilever. This yields a lumped-mass equation of motion for the system given by

$$\ddot{w} + 2\zeta\omega_n\dot{w} + (\omega_n^2 + \Delta\phi\lambda_1 + \Delta\phi^2\gamma_1)w + (k_2 + \Delta\phi\lambda_2)w^2 + (k_3 + \Delta\phi\lambda_3 + \Delta\phi^2\gamma_3)w^3 + \chi(w\dot{w}^2 + w^2\ddot{w}) = \eta_1\Delta\phi. \tag{8}$$

The nondimensional coefficients in Eqn. (8) are strong functions of the system's geometry, resonant modeshapes, and constituent material properties. The effective linear, quadratic, and the cubic stiffnesses (ω_n^2, k_2, k_3), and the nonlinear

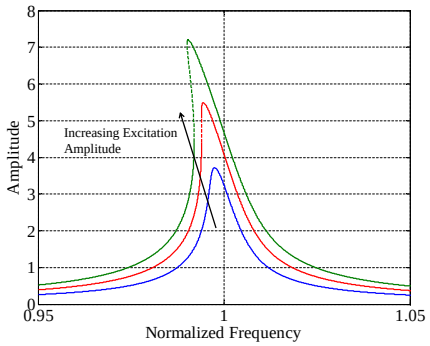

Figure 3: Simulated nonlinear frequency response of a representative piezoelectrically-actuated cantilever. The frequency response exhibits further softening as the excitation amplitude is increased.

term (χ) vary strongly with system's geometry and elastic material properties and exhibit a weak dependence on material nonlinearities. In contrast, the other terms in the expression are strong functions of the linear and nonlinear piezoelectric material coefficients. Note that though nonlinear constitutive relations were used to develop this model, if the constitutive relations are assumed to be linear, the system resembles a classic Duffing resonator. Detailed expressions for each of the terms presented here are omitted for the sake of brevity.

Equation (8) is highly nonlinear and fails to feature a tractable closed-form solution. Accordingly, the equation is analyzed using a numerical continuation program, AUTO [19]. This preliminary analysis is carried out by assuming that all the nonlinear material coefficients, with the exception of α_1, are zero. This follows the approach previously detailed in [17]. Figure 3 depicts the frequency response structure associated with the system, under various excitation amplitudes, for a representative value of α_1. As evident at comparatively-large excitation amplitudes, the system exhibits a softening-like behavior, with coexistent stable solutions and hysteresis. Accordingly, if the system is excited at a comparatively-low excitation frequency and frequency is swept to a higher value, the response amplitude will slowly increase until the excitation frequency crosses the (lower) point at which the stable and unstable solution branches meet (a saddle-node bifurcation). At this point, the response amplitude jumps to the large-amplitude response from the low amplitude state, and then decreases with increasing excitation frequency. In contrast, if the system is excited at a comparatively high excitation frequency and frequency is swept to a lower value, the response amplitude will rapidly increase until the excitation frequency crosses the (upper) point at which the stable and unstable solution branches meet (a second saddle-node bifurcation). At this point, the response amplitude jumps to the small-amplitude response from the high amplitude state, and then decreases with decreasing excitation frequency.

2.1 Bifurcation-Based Mass Sensing

As previously noted, in a traditional linear resonance based mass sensor, chemomechanically-induced shifts in the system's resonance frequency are tracked and used to signal an analyte detection event. In contrast, the proposed bifurcation-based resonant mass sensors exploit the rich nonlinear frequency response structure detailed above. Specifically, these sensors are designed to operate near the saddle-node bifurcation point designated A in Fig. 1(b). As with linear sensors, chemomechanical interactions with a target analyte are used to alter the effective mass of the resonator. However, in this instance, the added mass serves to not only shift the system's natural frequency, but also to drive the system across the saddle-node bifurcation. This yields a rapid and dramatic jump in the system's response amplitude which can be easily detected, even in the absence of significant readout electronics.

3 Experimental Investigation

To validate the feasibility and merits of the proposed nonlinear, bifurcation-based mass sensors a succinct experimental investigation was initiated. To begin, the nonlinear frequency response behavior of a representative device was characterized via laser vibrometry. Select microcantilevers were then selectively functionalized and tested within a carefully controlled environment using a custom test apparatus. Veeco DMASP probes, initially designed for use in scanning probe microscopy applications, were used as a test platform. These devices consist of a silicon cantilever and an integrated piezoelectric actuator incorporating a ZnO layer sandwiched between two Au/Ti electrodes.

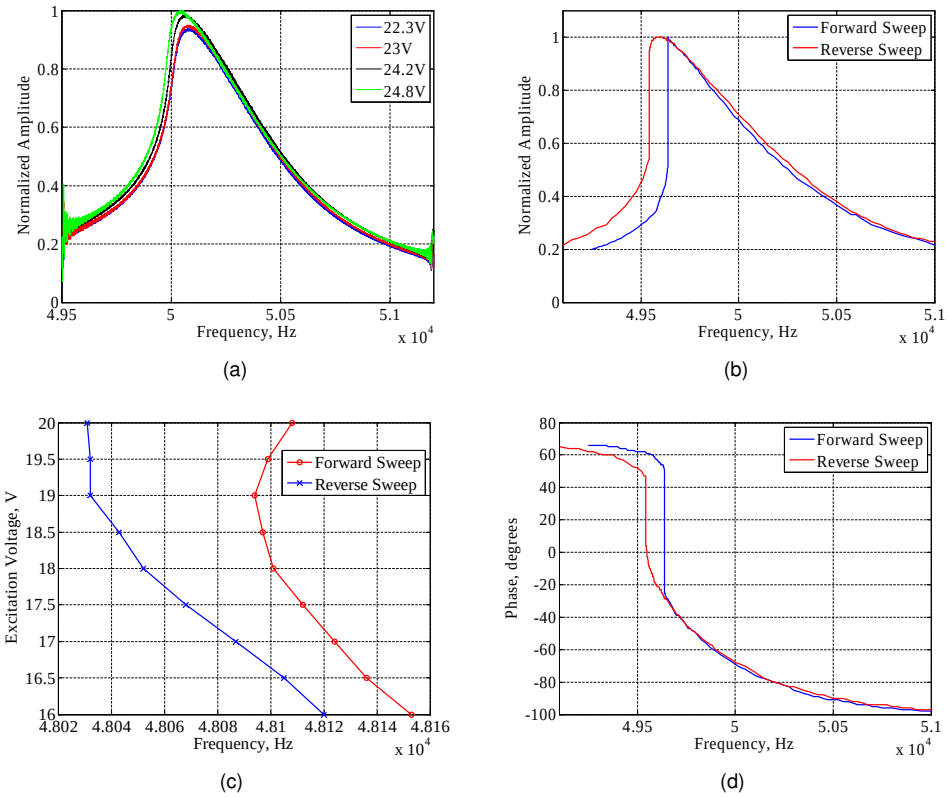

Figure 4: (a) Frequency response of the system under different excitation voltages. In this subfigure, 20.48 second sweep times were utilized. Note that the response becomes increasingly nonlinear as the excitation voltage is increased. (b) and (d) Amplitude and phase responses recovered with a 20.2 V_{pp} excitation using a total sweep time of 400 seconds. Note the clear bifurcations and hysteresis. Individual data points have been removed from the plot for the sake of clarity. (c) Relationship between the system's bifurcation frequencies and the amplitude of the excitation voltage. Though slightly problematic from an implementation point-of-view, the strong dependence of the bifurcation frequencies on the amplitude of excitation can be exploited for device tuning and performance metric optimization.

3.1 Nonlinear Frequency Response

The frequency response of the Veeco DMASP probes was studied through the use of a Polytec MSA-400 Laser Doppler Vibrometer and a supplementary LabVIEW interface, which served to control the voltage input and record the steady-state frequency response characteristics of the device. Frequency sweeps were performed at a variety of sweep rates and actuation voltage levels to characterize the nonlinear response of the microcantilevers. Figures 4(a) and 4(b) highlight the recovered amplitude response characteristics. The results depicted in Fig. 4(a) were recovered using a sweep period of 20.48 seconds (Note that this sweep rate is sufficiently fast that the saddle-node bifurcation is captured only in passing). As predicted, the system shows a mild softening behavior and the response increasingly softens with increasing excitation voltage. Similarly, Figs. 4(b) and 4(d) highlight the amplitude and phase response of the system recovered with 20.2 V_{pp} excitation and a 400 second sweep period. As evident, with higher sweep periods, even at a lower voltage, the system exhibits a clear saddle-node bifurcation and significant hysteresis.

3.2 Functionalization

Resonant mass sensors are typically functionalized with a polymer capable of adsorbing/absorbing solvents, vapors, and other analytes of interest [20]. Recently, inkjet technology has been shown to be a viable means of fabrication and sensor functionalization due to its ability to precisely deposit a small volume of liquid onto a substrate [21]. The benefits of this method are its high throughput, low production cost, ability to print a wide variety of liquids onto planar and non-planar surfaces, and environmental cleanliness, compared to conventional fabrication techniques [22].

In the present effort, the beams were functionalized with Poly 4-Vinyl Pyridine to facilitate methanol sensing [23].

Functionalization was carried out using a micro-inkjet printing process with thermal actuation enabled drop formation [24]. In this functionalization process, a resistor is placed within the polymer reservoir. An electrical current is sent through the resistor causing its temperature to rise. The resistor's temperature rises until a vapor bubble forms and subsequently collapses. This induces a wave in the fluid, which, in turn, results in the formation of a drop [25]. The inkjet system used for functionalizing the cantilevers is depicted in Fig. 5(a). It comprises of (a) a two-axis linear stage with an encoder resolution of 0.5 μm, (b) an HP TIPS thermal inkjet drop ejection system with printheads consisting of up to 18 nozzles with the ability to produce drop volumes in the range of 1-220 pL at a frequency of 45 kHz, (c) a CCD imaging system for the visualization of drop deposition, and (d) a laser registration system used for mapping fixed substrate coordinates [22]. Each device was functionalized with 110 pL drops in less than 1 second. The functionalized beams were stored in a nitrogen environment to avoid the interactions with free radicals and to ensure the integrity of the sensor's surface chemistry prior to testing.

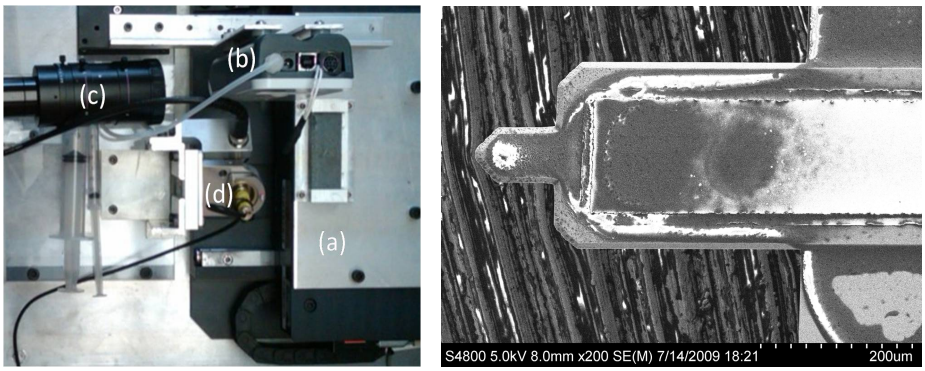

(a) (b)

Figure 5: (a) The micro-inkjet printing setup used for functionalization. (b) A scanning electron micrograph of the functionalized microcantilever.

3.3 Mass Sensing Trials

Once the nonlinear behavior of the resonant microcantilevers had been validated and deemed suitable for sensing, and the probes had been properly functionalized, laboratory-based sensing trials were initiated. The chemical test setup used for this study is depicted in Fig. 6. This test apparatus consists of multiple analyte bubblers, which are connected to precision mass flow controllers and a carrier gas (nitrogen) supply. The temperatures of the bubblers are carefully monitored and controlled through the use of RTDs and adjacent heat pads. By controlling the pressure of the carrier gas at the inlet, choosing appropriate temperature settings, and selecting appropriate flow rates for each of the mass flow controller, any desired analyte/carrier mixture and associated concentration level can be produced. Once fully mixed, this gas is diverted into a isolated test chamber inside of which the functionalized microbeams are mounted. The test chamber is optically accessible from the top, and features a glass window which is specially coated to allow for maximum transmission of the laser signal from the vibrometer. The temperature of the test chamber is also monitored and controlled using RTDs and heat pads to avoid the condensation of analyte onto the walls of the chamber and the optical viewport. Hermetically sealed electrical outlets are located at the base of the chamber to minimize interference with chemomechanical interactions. The exhaust from the chamber is routed into a condensing chamber from which the target analyte is recovered. The entire setup, including the excitation signal to the beam and recovered signal from the vibrometer, is monitored and controlled using a LabVIEW interface.

To validate the performance of the functionalized Veeco DMASP probes and the chemical test chamber itself, the microcantilevers were subjected to a series of mass sensing trials based on their linear frequency response. Specifically, the cantilevers were excited using a 2 V pseudorandom signal. Methanol was then supplied at a pre-determined concentration and rate into the chamber. To achieve successive adsorption and desorption of the gas molecules on the functionalized surface, the methanol/nitrogen mixture was supplied for a fixed period of time and then the system was purged with pure nitrogen. This alternating cycle of gas supply was controlled via LabVIEW. As previously noted, in a linear resonant mass sensor, as the mass is adsorbed on the surface, the natural frequency decreases, and as the mass desorbs, the natural frequency increases. As evident from Fig. 7 the expected behavior was recovered, albeit with comparatively large analyte/carrier concentrations (3.5% by mass). Current experiments are focused on validating the proposed nonlinear

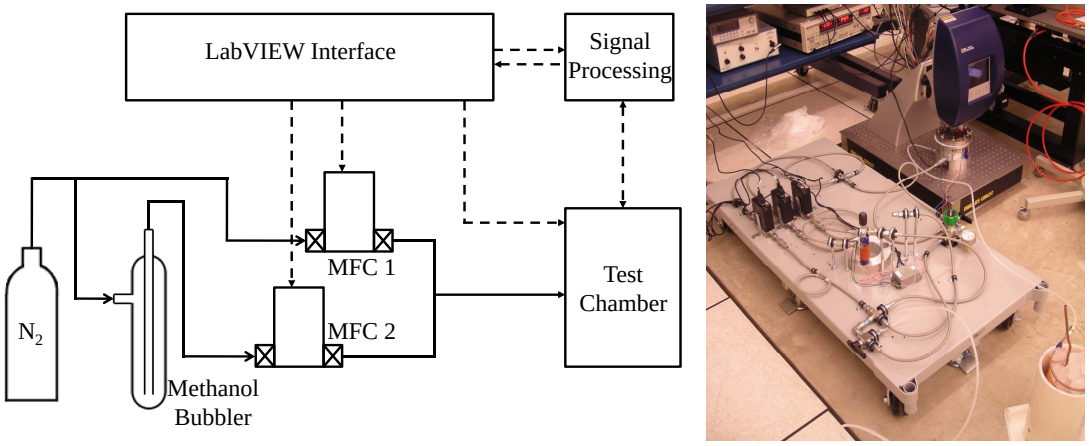

Figure 6: (a) Schematic and (b) pictorial representation of the computer-controlled chemical test apparatus.

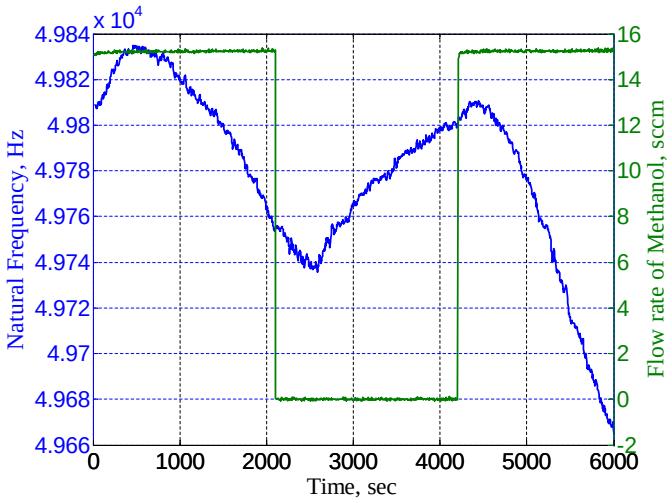

Figure 7: Preliminary linear resonant mass sensing results.

bifurcation-based sensing approach. Initial results have displayed significant promise.

4 Conclusions

The present work details the ongoing development of linear and nonlinear, bifurcation-based mass sensors based on piezoelectrically-actuated microresonators. A detailed nonlinear model for a representative microcantilever has been developed and analyzed to provide a high-level understand of pertinent system dynamics. Nonlinear behaviors deemed suitable for bifurcation-based sensing were experimentally verified using Veeco DMASP probes in conjunction with laser vibrometry. Select probes were functionalized using micro-inkjet techniques and initial experimental trials were completed to validate the integrity of the experimental approach. Current efforts are focused on validating the proposed nonlinear bifurcation-based sensing approach through further experimental investigation. Initial results have been quite promising.

References

[1] Thundat, T., Wachter, E. A. ,Sharp, S. L., and Warmack, R. J., "Detection of mercury vapor using resonating micro-cantilevers," *Applied Physics Letters*, vol. 66, no. 13, pp. 1695–1697, 1995.

[2] Ono, T., Li, X., Miyashita, H., and Esashi, M., "Mass sensing of adsorbed molecules in sub-picogram sample with ultrathin silicon resonator," *Review of Scientific Instruments*, vol. 74, no. 3, pp. 1240–1243, 2003.

[3] Lavrik, N. V. and Datskos, P. G., "Femtogram mass detection using photothermally actuated nanomechanical resonators," *Applied Physics Letters*, vol. 82, no. 16, pp. 2697–2699, 2003.

[4] Ekinci, K. L., Huang, X. M. H., and Roukes, M. L., "Ultrasensitive nanoelectromechanical mass detection," *Applied Physics Letters*, vol. 84, no. 22, pp. 4469–4471, 2004.

[5] Yang, Y. T., Callegari, C., Feng, X. L., Ekinci, K. L., and Roukes, M. L., "Zeptogram-scale nanomechanical mass sensing," *Nano Letters*, vol. 6, no. 4, pp. 583–586, 2006.

[6] Naik, A. K., Hanay, M. S., Hiebert, W. K., Feng, X. L., and Roukes, M. L., "Towards single-molecule nanomechanical mass spectrometry," *Nature Nanotechnology*, vol. 4, pp. 445–450, 2009.

[7] Lang, H. P., Berger, R., Battiston, F., Ramseyer, J.-P., Meyer, E., Andreoli, C., Brugger, J., Vettiger, P., Despont, M., Mezzacasa, T., Scandella, L., Guntherodt, H.-J., Gerber, C., and Gimzewski, J. K., "A chemical sensor based on a micromechanical cantilever array for the identification of gases and vapors," *Applied Physics A: Material Science & Processing*, vol. 66, supplement 1, pp. S61–S64, 1998.

[8] Nugaeva, N., Gfeller, K. Y. , Backmann, N., Lang, H. P., Duggelin, M., and Hegner, M., "Micromechanical cantilever array sensors for selective fungal immobilization and fast growth detection," *Biosensors and Bioelectronics*, vol. 21, no. 6, pp. 849–856, 2005.

[9] Su, M., Li, S., and Dravid, V. P., "Microcantilever resonance-based DNA detection with nanoparticle probes," *Applied Physics Letters*, vol. 82, no. 20, pp. 3562–3564, 2003.

[10] Boisen, A., Thaysen, J., Jensenius, H., and Hansen, O., "Environmental sensors based on micromachined cantilevers with integrated read-out," *Ultramicroscopy*, vol. 82, no. 1-4, pp. 11–16, 2000.

[11] Senesac, L., and Thundat, T. G., "Nanosensors for trace explosive detection," *Materials Today*, vol. 11, no. 3, pp. 28–36, 2008.

[12] Gurjar, M. and Jalili, N., "Toward ultrasmall mass detection using adaptive self-sensing piezoelectrically driven microcantilevers," *IEEE/ASME Transactions on Mechatronics*, vol. 12, no. 6, pp. 680–688, 2007.

[13] Wolf K., and Gottlieb, O., "Nonlinear dynamics of a noncontacting atomic force microscope cantilever actuated by a piezoelectric layer," *Journal of Applied Physics*, vol. 91, no. 7, pp. 4701–4709, 2002.

[14] Dai, M., Eom, K., and Kim, C.-W., "Nanomechanical mass detection using nonlinear oscillations," *Applied Physics Letters*, vol. 95, no. 203104, 2009.

[15] Younis, M. I. and Alsaleem, F., "Exploration of new concepts for mass detection in electrostatically-actuated structures based on nonlinear phenomena," *Journal of Computational and Nonlinear Dynamics*, vol. 4, no. 2, 021010, 2009.

[16] Postma, H. W. C., Kozinsky, I., Husain, A., and Roukes, M. L., "Dynamic range of nanotube- and nanowire-based electromechanical systems," *Applied Physics Letters*, vol. 86, no. 223105, 2005.

[17] Mahmoodi, S. N., Jalili, N., and Daqaq, M. F., "Modeling, nonlinear dynamics, and identification of a piezoelectrically actuated microcantilever sensor," *IEEE/ASME Transactions on Mechantronics*, vol. 13, no. 1, pp. 58-65, 2008.

[18] Joshi, S. P., "Non-linear constitutive relations for piezoceramic materials," *Smart Materials and Structures*, vol. 1, no. 1, pp. 80–83, 1992.

[19] Doedel, E., Champneys, A., Fairgrieve, T., Kuznetsov, Y., Sandstede, B., and Wang, X., "Auto 97: Continuation and bifurcation software for ordinary differential equations," 1997.

[20] Baller, M. K., Lang, H. P., Fritz, J., Gerber, C., Gimzewski, J. K. , Drechsler, U., Rothuizen, H., Despont, M., Vettiger, P., Battiston, F. M., Ramseyer, J. P., Fornaro, P., Meyer, E., and Guntherodt, H.-J., "A cantilever array-based artificial nose," *Ultramicroscopy*, vol. 82, no. 1, pp. 1–9, 2000.

[21] Calvert, P., "Inkjet printing for materials and devices," *Chemistry of Materials*, vol. 13, no. 10, pp. 3299–3305, 2001.

[22] Boley, W., Bhuvana, T., Hines, B., Sayer, R., Chiu, G.-C., Fisher, T., Bergstrom, D., Reifenberger, R., and Kulkarni, G., "Inkjet printing involving palladium alkanethiolates and carbon nanotubes functionalized with single-strand DNA," in *Proceedings of the DF2009: Digital Fabrication Processes Conference*, (Louisville, Kentucky), pp. 824–827, 2009.

[23] DeMartini, B. E., Rhoads, J. F., Zielke, M. A., Owen, K. G., Shaw, S. W., and Turner, K. L., "A single input-single output coupled microresonator array for the detection and identification of multiple analytes," *Applied Physics Letters*, vol. 93, no. 5, 054102, 2008.

[24] Post, N. J., *Precision Micro-Deposition of Functional Layers Using Inkjet Drop-on-Demand and Applications to the Functionalization of Microcantilever Sensors*. MS thesis, 2007.

[25] Lee, E., *Microdrop Generation*. CRC Press, 1st ed., 2003.